MAGNETIC CLEANLINESS AND THERMOMAGNETIC EFFECT: CASE STUDY OF THE ABSOLUTE SCALAR MAGNETOMETER AND ITS ENVIRONMENT ON SWARM SATELLITES

T. Jager[1,2], J. M. Léger[1,2], I. Fratter[3], P. Lier[3] and P. Pacholczyk[3]
[1]*Université Grenoble Alpes, Grenoble, France, Email:thomas.jager@cea.fr*
[2]*CEA, LETI, MINATEC Campus, Grenoble, France*
[3]*Centre National d'Etudes Spatiales (CNES), Toulouse, France*

ABSTRACT

This paper first summarizes the thermomagnetic effects highlighted during the magnetic verification and qualification campaign of the Absolute Scalar Magnetometer (ASM), the scalar reference instrument on board the ESA Swarm satellites launched on 22/11/2013 [1].
The physics of the thermomagnetic effect in metals is next reviewed. The physical and geometrical parameters affecting both the amplitude and the localization of the perturbations are detailed for objects of basic shapes and made out of one metal only. A predictive model has finally been developed and experimentally validated for simple geometrical and thermal configurations.

1. INTRODUCTION

As a part of common and standard development processes, all satellites and missions including magnetometers for scientific measurements have to go through extensive magnetic cleanliness verification and test programs. Well-known design rules shall be applied first and then the magnetic cleanliness of each spacecraft is checked and their magnetic properties are characterized [2-3]. During this process the remaining perturbation sources onto the magnetic instruments can thus be identified and reduced to the lowest achievable level, the remaining effects being then characterized for post process corrections: the remanent, induced and other spacecraft-system generated magnetic perturbations are characterized on ground at the requested accuracy level in dedicated facilities before launch [4]. Additional effects are also to be taken into account, in particular the thermoelectric effects generated by thermal gradients or heat flows which are difficult both to predict and to evaluate in representative conditions. These effects, which are thus complex to handle and to get rid of, can even occur with single metallic material parts [5] commonly used in structural items for their low or non-magnetic properties such as aluminum or titanium.
In the first part of this paper, a specific focus will be given on this thermomagnetic effect illustrated by the tests performed during the magnetic verification and qualification campaign of the ASM instrument. In a second part, the thermomagnetic effect in metal is reviewed: a predictive perturbation model is built based on [5] and then experimentally validated for simple geometrical and thermal configurations.

2. CHARACTERIZATION AND REMOVAL OF THERMOMAGNETIC PERTURBATIONS ONTO ASM INSTRUMENTS

2.1. First characterizations

As the magnetic reference sensor on-board Swarm satellites, the ASM sensors had to go through an extensive magnetic qualification campaign, from standalone qualifications tests [6], tests performed with several platform interface elements up to final tests performed on the satellites once integrated [4]. The last ones did show unexpected thermomagnetic perturbations, in the 10 nT range, generated when the platform heaters dedicated to the ASM thermal control (located on the interface bracket between the ASM and the tip of the satellite boom) were activated (cf Figure 1 for hardware configuration details). Since it had been previously verified that the heaters did not generate any direct magnetic perturbations themselves, these tests pointed out indirect perturbations (i.e. current loops) generated by the thermal gradients set in the titanium interface bracket.

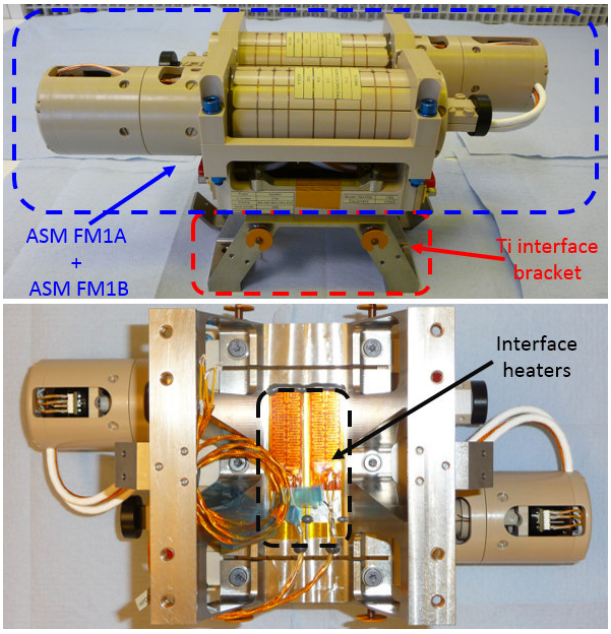

Figure 1. ASM and its initial interface bracket configuration (side and bottom views).

2.2. Perturbation removal strategy

A step-by-step perturbation identification and removal process has then been set up in order to characterize the global perturbation and has resulted in several hardware upgrades. Thanks to dedicated scalar differential measurements performed in the CEA-Leti Magnetic Characterization Facility of Herbeys, all elements which have been characterized as sources of thermomagnetic perturbations have been progressively removed or replaced. An example of a test set-up is given on Figure 2 where an {ASM + interface bracket} assembly, including heaters, is operated and characterized in different orientations: the ASM scalar measurements are directly compared to the ones of several reference magnetometers (here Nuclear Magnetic Resonance sensors) operated in the ambient magnetic field few meters away from the ASM. The resulting scalar differentials are then analysed in relationship with the operating cycle of the heaters to characterize the perturbations onto the ASM, if any.

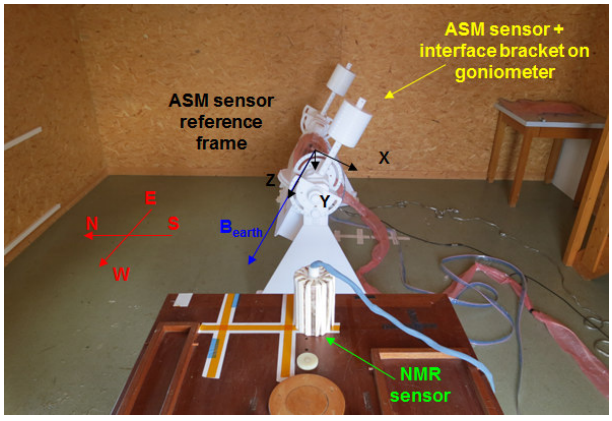

Figure 2. Example of scalar differential test Set-up in one of the amagnetic test cabins of Herbeys

2.3. Results

The aforementioned test process has led to several hardware upgrades (3 in total, cf Figure 3) of both the mechanical interface of the ASM with the satellite boom and later even some ASM components. The original titanium interface bracket including the heaters for the ASM thermal control has been replaced by CFRP (Carbon Fiber Reinforced Polymer) components and the ASM internal harness connectors have been removed. These successive evolutions can be simply summarized as follows: the less metallic material submitted to thermal gradient in the vicinity of the ASM, the smaller the perturbation, which makes perfectly sense with thermomagnetic generated effects.

In the end, this exhaustive test campaign has demonstrated the very efficient reduction of thermomagnetic perturbations generated in the close environment of the ASM: the remaining maximum effects have been characterized in the 20-30 pT +/- 5 pT peak-to-peak range (cf Figure 4) which is well below

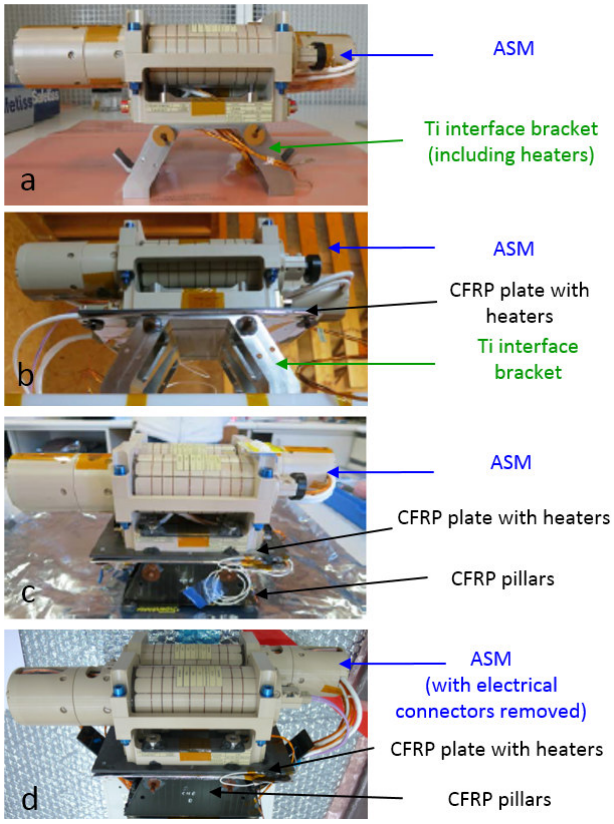

*Figure 3. The {ASM + mechanical boom interface} configurations: the original one (**a**), the 2 intermediate (**b**, **c**) and the final one (**d**)*

the accuracy specification of 300 pT (2σ) allowed for ASM for the Swarm mission [1].

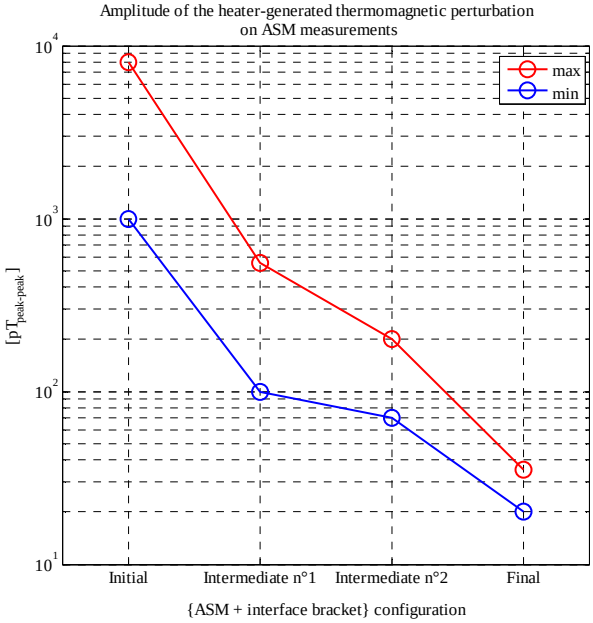

Figure 4. Amplitude of the heater-generated thermomagnetic perturbation on the ASM sensor w.r.t assembly configuration

(measurement accuracy of +/- 5 pT)

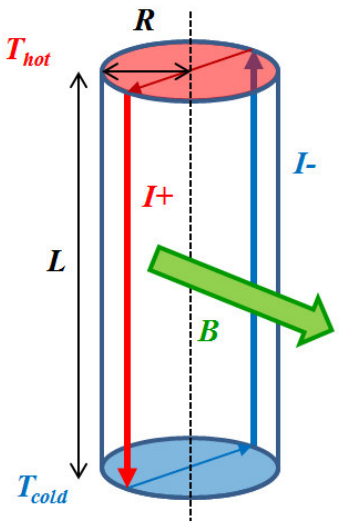

Figure 5. Thermomagnetic current loop generated by longitudinal thermal gradient in a cylinder rod

3. UNDERSTANDING THE THERMOMAGNETIC EFFECT

3.1. The physics behind the thermomagnetic effect

The physics of the thermomagnetic effect in metals is here reviewed on the basis of [5]: as illustrated on the Figure 5, when a cylindric metallic rod is submitted to a uniform longitudinal temperature gradient, a current loop is set, originating from two opposite electronic current flows *I*+ and *I*-.The thermalization current from the hot to the cold side due to heat transfer, *I*+, is described in [5] with a combination of Sommerfeld and Debye models for a gas a free electrons in metals while the reverse current from the cold to the hot side *I*-, is created by the internal Seebeck electric field resulting from the *I*+ current. In [5] it is stated that due to electromagnetic interaction, the *I*+ and *I*- currents repel each other at diametrically opposite sides of the cylinder, generating a magnetic moment and a magnetic field which can be detected afterwards with a proper test set-up including magnetic sensors. This physical model is supported and validated by experiments in [5]: for a given thermal configuration, the amplitude of the generated magnetic field fits with the physical model description, the location of the current loop being fixed once and for all in the cylinder. However, its initial orientation w.r.t. the cylinder axis remains unknown before testing and seems driven by internal defects locations and geometrical imperfections at small scales in the tested materials.

3.2. Thermomagnetic model building and validation strategy

In order to get a better understanding of the previously detailed thermally-generated magnetic perturbations observed on the ASM measurements throughout the different {ASM + interface bracket} configurations, we decided to adapt and to validate the model of reference [5] in case of simple geometrical configurations and for all the bulk materials which have been used in the different hardware configurations.

The model of the thermomagnetic perturbation has been first extrapolated from [5] in case of cylinder rods long enough so that the magnetic perturbation can been seen as the sum of the magnetic fields generated by two infinite wires carrying the *I*+ and *I*- currents. The amplitude *I* of these two currents is here given by (1):

$$I = \frac{\pi \kappa R^2}{6} \frac{e}{k_B} \frac{T_D^3}{T_F^2} \left(\frac{\nabla T}{T^2} \right) \qquad (1)$$

where R is the cylinder radius, κ is the material thermal conductivity, e is the electronic elementary charge, k_B is the Boltzmann constant, T the ambient temperature, ∇T the longitudinal thermal gradient (i.e $(T_{hot}\text{-}T_{cold})$ /L) and T_F and T_D respectively the material Fermi and Debye temperatures.
The resulting magnetic field at a given position is obtained by adding the separate contributions of *I*+ and *I*-, each one being approximated by (2):

$$\vec{B}_{wire}(I, r) = \frac{\mu_0 I}{2\pi r} \vec{u}_\theta \qquad (2)$$

The maximum magnetic field B generated at the cylinder interface, orthogonal to the internal current loop plane is then given by (3):

$$B_{\max} = \frac{\mu_0 \kappa R}{12} \frac{e}{k_B} \frac{T_D^3}{T_F^2} \left(\frac{\nabla T}{T^2} \right) \qquad (3)$$

The Table 1 gives the numerical results of this formula for 3 cm diameter cylinders of pure and space-grade aluminium and titanium alloys, submitted to a 20 K/m longitudinal gradient.

The order of magnitude of the calculated perturbations (in the nT range for Ti based configurations) due to a thermomagnetic effect as described in [5] is consistent with the thermally generated perturbations previously observed and detailed throughout the {ASM + interface bracket} testing.

To further validate this perturbation model, we have set-up a dedicated scalar differential test configuration, where a PFM ASM model was operated in the close vicinity of a rod submitted to a longitudinal thermal gradient. The second scalar reference sensor (here a

Material	T_F (K)	T_D (K)	κ ($Wm^{-1}K^{-1}$)	$B_{max}/\nabla T$ pT/ (K/m)	B_{max} (nT)
Al (pure)	134900	428	237	217	4.33
Al AU4G (2017A T3)	134900	428	134	122	2.45
Ti (pure)	83700	420	21.9	49	0.98
Ti grade V (TA6-V)	83700	420	6.7	15	0.30

Table 1. Material characteristics and calculated thermomagnetic perturbation for cylinder rods submitted to a 20 K/m longitudinal thermal gradient

NMR sensor) requested to perform the scalar differential measurement was operated a few meters away from the {rod + ASM} assembly. This configuration detailed on Figure 6 has been operated with different types of rods: different materials (also including insulating ones such as PEEK or CFRP used in both the ASM and the final interface bracket configurations), different radii and cross-sections (to check whether or not the loop location could be determined by geometrical design in case of non-circular cross-section).

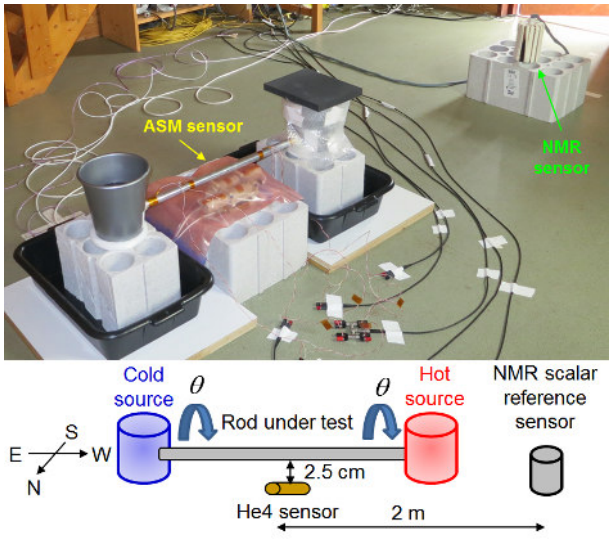

Figure 6. Scalar differential test set-up for the thermomagnetic model validation

Each rod is then tested as follows:

- The scalar differential and the longitudinal thermal gradient are recorded for an initial rod position when submitted to thermal excitation
- The measurement is then repeated for rod rotations by steps of 90 ° until a complete revolution has been achieved
- The results are then compared to the model predictions both in terms of perturbation amplitude and internal current loop orientation.

3.3. Tests results

Thermomagnetic current loops have been successfully generated for all metallic rods, in good agreement with the expected characteristics previously derived from the perturbation model. As an illustration the Figure 7 details the temporal evolutions of the ASM-NMR scalar differential and thermal gradient recorded for a given orientation in the case of a Ti grade V 3 cm circular cross-section rod. The derived perturbation model fit added to the plot is in good agreement with the measurements (first order polynomial fit between ∇T and the scalar differential evolution). The slight delay between magnetic and temperature measurements is attributed to the test configuration and the actual locations of the thermistors w.r.t the heat source.

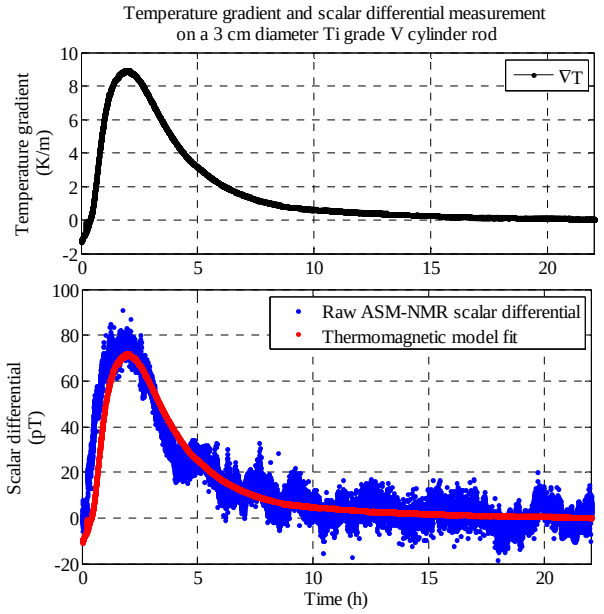

Figure 7. Respective evolutions of longitudinal thermal gradient and ASM-NMR scalar differential for a test performed on a ∅3cm Ti grade V rod

As expected, no signature has been observed for the insulating materials tested (CFRP, PEEK and alumina).

For all metallic elements, a fixed location of a current loop perturbation has been characterized and derived from the rotation measurements. This is illustrated on Figure 8 where the derived maximum amplitude perturbation coefficients in case of a ∅3cm Ti grade V rod are displayed as a function of the rod rotation angle and compared to the expected perturbation shape of a

Material		Aluminium AU4G (2017A T3)	Titanium grade 5 (TA6-V)	CFRP	Alumina (Al_2O_3)	PEEK
Rod diameter *R* (cm)		3	3	3	3	3
Maximum perturbation ($pT/K.m^{-1}$)	model	13.8 @2.5 cm	6 @2.5 cm	none	none	none
	measurement	16.5 @2.5 cm	10.9 @2.5 cm	none	none	none

Table 2. Maximum amplitude of the characterized thermomagnetic perturbation @ 2.5 cm for rods of different materials

rotated loop. Given the size and location of the helium cell of the ASM sensor, the loop perturbation model correctly predicts the generated perturbation projection onto the main ambient field seen by the He4 atoms of the gas cell.

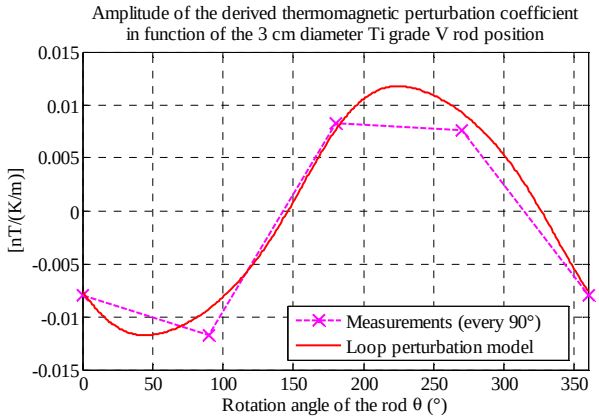

Figure 8. Measured and calculated thermomagnetic perturbation coefficient in function of the rotation angle for a ∅3cm Ti grade V rod

Even if the initial position of the current loop cannot be predicted in case of a circular cross-section rod, we have demonstrated that it can indeed be imposed in case of rectangular cross-sections : in order to minimize electromagnetic interactions between the *I+* and the *I-* currents, the loop will set-up in the plane containing the larger available rod cross-section (for example in case of a rectangular cross section with a high aspect ratio between width and height, the loop will set-up in the width plane).

The results of this thermomagnetic perturbation model validation study are summarized in Table 2:

- the perturbation model for metals is in good agreement with the measurements: the thermally generated magnetic perturbations observed with the first generations of {ASM + interface bracket} assembly can thus be well described and understood with the thermomagnetic effect
- as expected the insulating materials which constitute the main components of both the ASM and the final interface bracket are not subjected to thermomagnetic effects

4. CONCLUSION

In this paper we have been able to correlate with a good agreement the observations of thermally-generated magnetic perturbations in the close environment of the first generations of the {ASM + interface bracket} assembly to the thermomagnetic effect occurring in metals. Thanks to the removal and/or replacement of metallic components in the close environment of the ASM sensor, it has been possible to get rid of these perturbations before the launch of the Swarm satellites.
This study finally puts further emphasis on one of the basic design rules for the conception and integration of magnetic sensors on-board space vehicles: avoid as much as possible metallic elements in the vicinity of these instruments, even if they do not show any static magnetic signature. They can still give rise to magnetic perturbations if they are submitted to thermal gradients, which turn to be very difficult to compensate for by modelling as these elements are never simple in shape and as it also requires a very precise 3D knowledge of their internal temperature distribution.

5. REFERENCES

1. Friis-Christensen, E., Lühr, H., Hulot, G. (2006). Swarm: A constellation to study the Earth's magnetic field. *Earth, Planets and Space*, 53:351-358.

2. Acuña, M.H. (2004). The design, construction and test of magnetically clean spacecraft - A practical guide. *NASA/GSFC internal report*, Rev 3.0.

3. Assessment and control of spacecraft magnetic fields (1970). *NASA Space Vehicle Design Criteria technical report*, SP-8037.

4. Alcouffe, F., Bertrand, F., Jager, T., Le Prado, M., Léger, J.M., Fratter, I. (2012). The swarm absolute scalar magnetometer magnetic cleanliness program. *Proceedings ESA Workshop on Aerospace EMC*.

5. Vasiliev, B.V. (2014). The New Thermo-magnetic Effect in Metals. *Universal Journal of Physics and Application* 2(4), 221-225.

6. Jager, T., Léger, J.M., Bertrand, F., Fratter, I. and Lalaurie, J.C. (2010). SWARM Absolute Scalar

Magnetometer accuracy: analyses and measurement results. *Proceedings of the IEEE Sensors Conference*, 2392-2395.